

From a Relatively Hydrophobic and Triethylamine (TEA) Adsorption-Selective Core–Shell Heterostructure to a Humidity-Resistant and TEA Highly Selective Sensing Prototype: An Alternative Approach to Improve the Sensing Characteristics of TEA Sensors

Hao Fu, Hongyun Shao, Liwei Wang,* Han Jin,* Dehua Xia, Shengwei Deng, Yinghui Wang, Yi Chen, Changzhou Hua, Li Liu, and Ling Zang*



Cite This: *ACS Sens.* 2020, 5, 571–579



Read Online

ACCESS |



Metrics & More



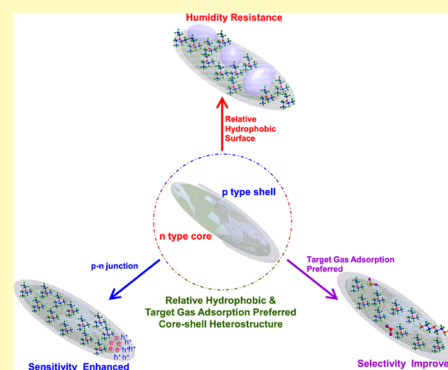
Article Recommendations



Supporting Information

ABSTRACT: During the detection of industrial toxic gases, such as triethylamine (TEA), poor selectivity and negative humidity impact are still challenging issues. A frequently reported strategy is to employ molecular sieves or metal–organic framework (MOF) membranes so that interference derived from surrounding gases or water vapor can be blocked. Nevertheless, the decline in the response signal was also observed after coating these membranes. Herein, an alternative strategy that is based on a hydrophobic, TEA adsorption-selective p–n junction core–shell heterostructure is proposed and is speculated to simultaneously enhance selectivity, sensitivity, and humidity resistance. To verify the practicability of the proposed strategy, a thickness-tunable nitrogen-doped carbon (N–C) shell-coated α -Fe₂O₃ nano-olive (N–C@ α -Fe₂O₃ NO)-based core–shell heterostructure that is obtained via a unique all-vapor-phase processing method is selected as the research example. After forming the core–shell heterostructure, a relatively hydrophobic and TEA adsorption-selective N–C@ α -Fe₂O₃ NO surface was experimentally confirmed. Particularly, a chemiresistive sensor that comprises N–C@ α -Fe₂O₃ NOs exhibits satisfactory selectivity and response magnitude to TEA when compared with the sensor using α -Fe₂O₃ NOs. The detection limit can even reduce to be 400 ppb at 250 °C. Furthermore, the sensor based on N–C@ α -Fe₂O₃ NOs shows desirable humidity resistance within the relative humidity (RH) range of 30–90%. For practical usage, a sensing prototype based on the N–C@ α -Fe₂O₃ NO probe is fabricated, and its satisfactory sensing performance further confirms the potential for future applications in industrial organic amine detection. These promising results show a bright future in enhancing the humidity resistance and selectivity as well as sensitivity of chemiresistive sensors by simply designing a hydrophobic and target gas adsorption (e.g., TEA) preferred p–n junction core–shell heterostructure.

KEYWORDS: hydrophobic core–shell heterostructure, N–C@ α -Fe₂O₃ nano-olives, TEA selective, humidity resistance, all-vapor-phase processing method



Triethylamine (TEA) is one of the most important organic materials used in the production process while it is a typical toxic,^{1,2} inflammable, and explosive industrial chemical. Exposure to TEA (≥ 10 ppm) can cause severe health problems,³ such as pulmonary edema, expiratory headache, comatose state, and eye irritation.^{4,5} Therefore, there is an urgent need to propose an effective and real-time sensing device for detecting TEA at trace levels, particularly in the area close to chemical plants. For the purpose of timely warning of the leakage of TEA, numerous chemical sensors have been explored for detecting TEA vapors in recent years, and most of them are based on metal oxide semiconductor (MOS) chemiresistive materials.^{6–8} Although promising advancements have been witnessed over the past decade, two major technical challenges, namely, poor selectivity and negative humidity effect, still remain for these MOS-based gas sensors. For

instance, the intrinsic sensitivity of metal oxides to moisture and/or other surrounding gases causes a significant signal fluctuation when humidity and/or the level of interfering gases changes,^{9,10} hindering their application in sensing TEA in real conditions.

To date, molecular sieves or metal–organic framework (MOF) coated sensing materials have been often reported for enhancing the selectivity and humidity resistance.^{11–14} Benefiting from the filter effect derived from the molecular sieves or MOF, negative interference is effectively eliminated.

Received: December 20, 2019

Accepted: February 4, 2020

Published: February 4, 2020

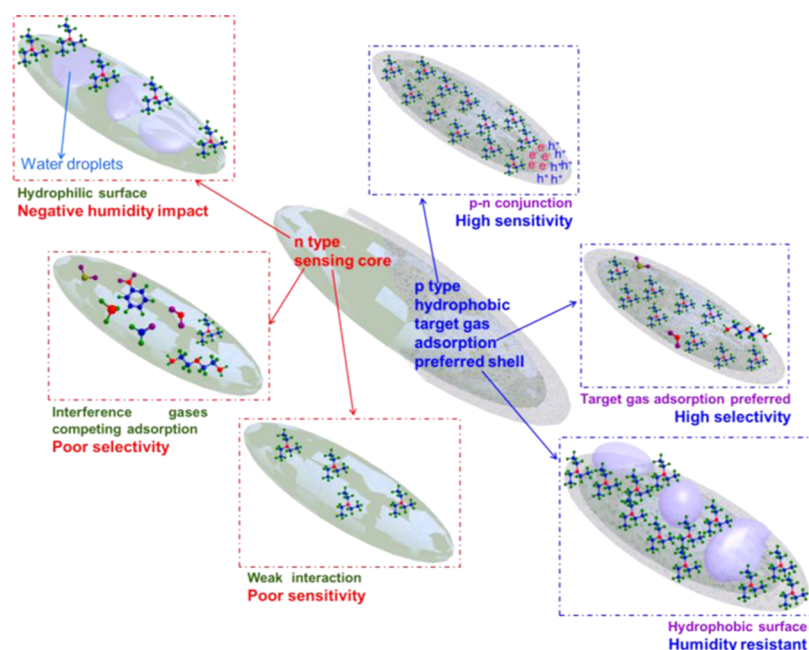


Figure 1. Illustration of the proposed strategy for selective and sensitive detection of the target gas with enhanced humidity resistance.

Nevertheless, these molecular sieves or MOF membranes also block part of the target gas molecules from reaching reaction sites, resulting in a decrease in the response signal. This is definitely unsuitable to detect analytes at low concentration. A p–n junction was often adopted to improve gas response, while it should be noted that a p–n junction for enhancing the humidity resistance is less reported.^{15–20} In a word, effectively declining the negative impact of water vapor while maintaining desirable response sensitivity and selectivity is still a concerned issue. An alternative strategy to address these problems is to construct sensing materials coated with a hydrophobic and target gas adsorption-selective porous membrane with controlled thickness to facilitate the diffusion and transmission of gas molecules, which enables both humidity resistance and high selectivity.^{1,21–23} Particularly, a p–n junction on the membrane-coated MOS is speculated to bring about significant enhancement in the response signal and sensitivity as well as low limit of detection (LOD).^{17,24–26} In comparison with those reported approaches that primarily rely on molecular sieves or MOF membranes, the strategy proposed in this article offers the opportunity of simultaneously enhancing selectivity, sensitivity, and humidity resistance as well as the low LOD via a more efficient and cost-effective way. Herein, the practicability of the proposed strategy will be experimentally verified by designing a hydrophobic and TEA adsorption-selective core–shell heterostructure. In addition, the sensing behavior of the chemiresistive sensor based on the proposed core–shell heterostructure will be systematically evaluated. Moreover, interrelationship between the enhanced sensing performance and the proposed strategy will be particularly focused and discussed in depth. Finally, a sensing prototype will be built and operated in real working conditions to further support the success of the proposed strategy.

EXPERIMENTAL SECTION

Preparation of N–C@ α -Fe₂O₃ Nano-Olives (NOs). The details of synthesizing α -Fe₂O₃ nano-olives (NOs) were described in the experimental details in the [Supporting Information](#). A certain amount

of the obtained α -Fe₂O₃ NOs was put onto the bottom of a smaller crucible. Then, the smaller crucible was placed upside down in a larger crucible as illustrated in [Figure S1](#) of the [Support Information](#). At the bottom of the larger crucible was evenly sprinkled an appropriate amount of melamine. Afterward, two sets of crucibles were heated in a muffle furnace at 550 °C for 2 h. During the thermal polycondensation process as reported previously,^{27,28} melamine sublimed and formed a uniform nitrogen-doped carbon shell (N–C) on the surface of an α -Fe₂O₃ NO product. For a reasonable comparison of sensor performance, the sample without N–C coating was also treated in the same way as the N–C-coated one but in the absence of melamine, and the treated sample is named as annealed α -Fe₂O₃ NOs to be distinct from the as-synthesized sample. Besides, to discuss the role and impact of the N–C shell on the gas sensing performance, various samples with different additive mass ratios of melamine to α -Fe₂O₃ NOs such as 1:1, 5:1, and 8:1 were used and denoted as N–C@ α -Fe₂O₃ NOs (3 nm), N–C@ α -Fe₂O₃ NOs (5 nm), and N–C@ α -Fe₂O₃ NOs (8 nm); wherein, 3, 5, and 8 nm represent the N–C shell thickness, respectively. More rigorous was that the mass ratio of melamine to α -Fe₂O₃ NOs as 10:1 had also been complemented to explain the quantitative change of shell thickness with the additive amount of melamine.

Materials Characterization. The samples were characterized by powder X-ray diffraction (XRD) analysis (Rigaku Ultima IV, Japan, Cu K α radiation, $\lambda = 1.5418$ Å), field-emission scanning electron microscopy (FESEM) (Hitachi SU5000, Japan), transmission electron microscopy (TEM), high-resolution TEM (HRTEM), and energy-dispersive X-ray spectroscopy (EDS) (FEI Tecnai G2 f20 s-twin, 200 kV), X-ray photoelectron spectroscopy (XPS) (Thermo SCIENTIFIC ESCALAB 250Xi, Al K α X-ray monochromator), contact angle (VCA Optima XE, AST Ltd.), Fourier transform infrared spectroscopy (FTIR) (IRTrace-100, SHIMADZU, Japan), thermogravimetric (TG)-FTIR (TGA 8000-FT-IR, PerkinElmer), ultraviolet photoelectron spectroscopy (UPS) (ESCALAB 250Xi, Thermo Fischer), and UV/Vis spectroscopy (PE 950, PerkinElmer).

Sensor Fabrication and Evaluation of Sensing Characteristics. The details of gas sensor fabrication and sensing test can be found in our previous works and part ii of experimental details in the [Supporting Information](#).²⁹ Sensing characteristics of the fabricated sensors were evaluated by a CGS-8 intelligent test system (Beijing Elite Tech Co. Ltd., China), which provides precise control of gas flow and dilution, measurement of electrical resistance ([Figure S2](#) of the [Supporting Information](#)). Initially, dry air was used as the

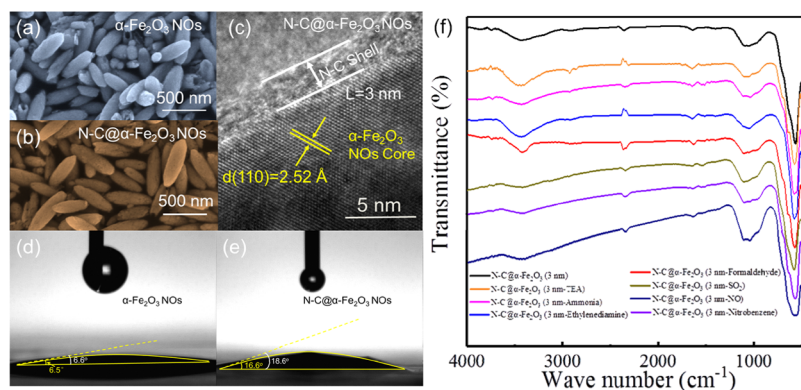


Figure 2. FESEM images of (a) α -Fe₂O₃ NOs and (b) N-C@ α -Fe₂O₃ NOs (3 nm) and (c) HRTEM image of the interfacial layer of N-C@ α -Fe₂O₃ NOs (3 nm). The 3 nm shell makes the gas diffusion easier, avoiding the decrease in the response signal. Contact angle of (d) α -Fe₂O₃ NOs and (e) N-C@ α -Fe₂O₃ NOs (3 nm) with water. The relatively increased contact angle indirectly confirmed a relatively hydrophobic N-C shell, which is helpful to minimize the impact of humidity in sensing TEA; (f) FTIR spectrum of α -Fe₂O₃ NOs and N-C@ α -Fe₂O₃ NOs (3 nm) after exposure to 100 ppm TEA and other selected interfering gases. The extra peak appearing within the wave number range of 2800–3000 cm⁻¹ indicates the preferred adsorption of TEA on the N-C shell after N-C@ α -Fe₂O₃ NOs were exposed to TEA.

reference and diluted gas. Then, when investigating the impact of relative humidity (RH) on the sensing performance, a certain amount of water vapor had been premixed with TEA vapor and air at room temperature of 20 °C to reach specific RH. It should be noted that all RH measurements were performed at room temperature, and then the mixed gases were introduced into the test chamber of the CGS-8 intelligent test system. The sensor was heated by the Ni-Cr heating alloy to modulate the test temperatures from 150 to 350 °C. The sensor response is defined as $S = R_a/R_g$, where R_a is the sensor resistance in reference air and R_g is the sensor resistance when the target chemical is present.^{30,31} The response/recovery time is defined as the time required for a device resistance change to reach 90% of the total resistance change.³⁰ The variation of the response signal is presented by error bars.

RESULTS AND DISCUSSION

Figure 1 summarizes the general strategy of the research: (1) a sensing material with poor selectivity and sensitivity to TEA is selected as the “core” candidate and experimental control, since the research objective of the study is to clarify the impact of a hydrophobic and TEA adsorption-selective “shell”; (2) a hydrophobic and TEA adsorption-selective shell is coated on the surface of the core to form a core-shell heterostructure. In light of the fact that a hydrophobic surface is unfavorable to adsorb water vapor, it is deduced that TEA adsorption should dominate the whole sensing process. In other words, high selectivity to TEA against other interfering gases (including water vapor) is speculated; (3) due to the fact that a p-n junction is usually formed the core-shell heterostructure and is beneficial to improving the response magnitude, significant improvement in the sensitivity and LOD is expected. To verify the practicability of the proposed strategy, the following steps are implemented: owing to the fact that a minor response magnitude and poor selectivity to TEA were observed in our pilot study, α -Fe₂O₃ NOs are selected as the core material in the research. Besides, as a metal-free nitrogen-doped carbon (N-C) nanofilm has been frequently used as surface coating to raise the catalytic activity of MOS materials,^{32,33} a N-C nanofilm is selected as the shell candidate, as these N-C-coated composite materials exhibit better adsorption property, larger specific surface area, and faster electron-transport property.^{21,34–37}

α -Fe₂O₃ NOs and N-C@ α -Fe₂O₃ NOs (3 nm) were synthesized via a conventional hydrothermal route and a

unique all-vapor-phase processing method, respectively. Details of material characterization and relevant discussion can be found in the Materials Characterization section in the Supporting Information. In brief, the global surface morphology of α -Fe₂O₃ NOs presents no significant difference after N-C shell coating, shown in Figures 2a,b and S3 of the Supporting Information. The thickness of the N-C shell is roughly estimated to 3 nm (Figure 2c), which is favorable for gas diffusion. X-ray diffraction (XRD) patterns shown in Figure S4 of the Supporting Information suggest a pure α -Fe₂O₃ phase (JCPDS No. 33-0664) for the obtained α -Fe₂O₃ NOs,^{38,39} no matter heat-treated or not. Nevertheless, owing to the reducing action of the N-C shell, a small amount of γ -Fe₂O₃ is likely to be witnessed in the sample of N-C@ α -Fe₂O₃ NOs (3 nm).⁴⁰ It must be noted that since only a small amount of γ -Fe₂O₃ is observed in the sample, response behavior of N-C@ α -Fe₂O₃ NOs (3 nm) will be hardly affected. X-ray photoelectron spectroscopy (XPS) results shown in Figure S5 of the Supporting Information confirm the success of coating the N-C shell on the surface of α -Fe₂O₃ NOs. Furthermore, changes in the binding energy support the strong interfacial interaction between the N-C shell and α -Fe₂O₃ NOs.

Since the hydrophobic and TEA adsorption-selective shell is crucial to achieve humidity resistance and TEA selectivity, the contact angle of water droplets and gas adsorption on the surface of α -Fe₂O₃ NOs and N-C@ α -Fe₂O₃ NOs (3 nm) were studied and compared. Figure 2d,e demonstrates the contact angle of water droplets on each sensing material. It can be concluded that a hydrophilic surface can be assigned to α -Fe₂O₃ NOs due to the low value of contact angle (around 6.5°). In contrast, a relatively hydrophobic surface is speculated for N-C@ α -Fe₂O₃ NOs (3 nm) owing to the minor increase in the contact angle (18.6°). In view of the fact that a relatively hydrophobic surface may result in more difficulties in adsorbing water vapor on the surface and leaving more reaction sites to target gases, it is reasonable to assume that some part of humidity resistance would be demonstrated by N-C@ α -Fe₂O₃ NOs (3 nm). Regarding the TEA adsorption capability of N-C@ α -Fe₂O₃ NOs (3 nm), theoretical calculations could be helpful to give a theoretical guidance. However, the theoretical calculation cannot be done

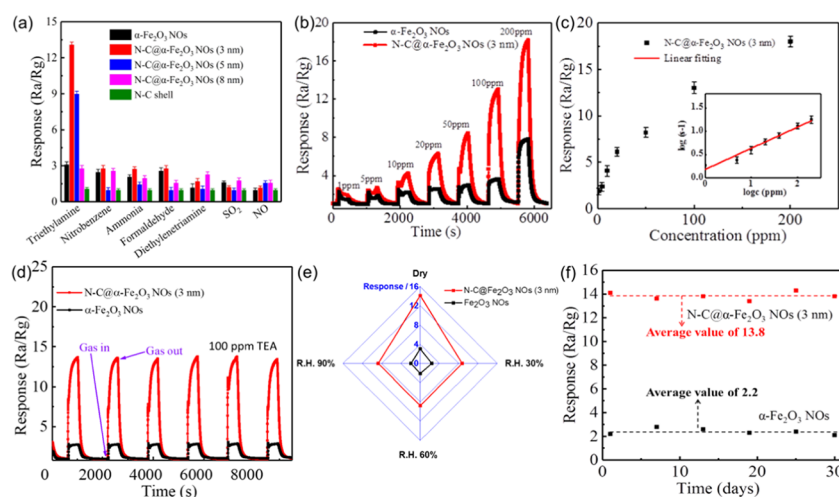


Figure 3. (a) Cross-sensitivity of the sensors composed of α -Fe₂O₃ NOs, N-C@ α -Fe₂O₃ NOs (3 nm), N-C@ α -Fe₂O₃ NOs (5 nm), N-C@ α -Fe₂O₃ NOs (8 nm), and N-C shell. Optimal selectivity and response magnitude are observed for the sensor consisting of N-C@ α -Fe₂O₃ NOs (3 nm); (b) transient responses and (c) dependence of the response signal on TEA concentration in the range of 1–200 ppm for the sensor using N-C@ α -Fe₂O₃ NOs (3 nm) (as the sensing material); (d) variation of the response signal with the changing humidity for the sensors composed of α -Fe₂O₃ NOs and N-C@ α -Fe₂O₃ NOs (3 nm). Identical response magnitude to 100 ppm of TEA is witnessed for the sensor using N-C@ α -Fe₂O₃ NOs, within the humidity of 30–90%; (e) impact of the water vapor in the relative content (RH) of 0 (dry)–90% on the response magnitude of the sensor using α -Fe₂O₃ NOs and N-C@ α -Fe₂O₃ NOs (3 nm); (f) response stability of the sensors composed of α -Fe₂O₃ NOs and N-C@ α -Fe₂O₃ NOs (3 nm), operated at 250 °C for almost 1 month. Minor changes are observed for the developed sensor, indicating acceptable long-term stability in real applications.

in this research because of the amorphous N–C membrane presented in the article and the theoretical calculation (e.g., density functional theory) can only be adopted for the materials with well-crystallized microstructures. Herein, a Fourier transform infrared spectrometer (FTIR) was employed, and the FTIR spectrum is shown in Figure 2f. Obviously, after N-C@ α -Fe₂O₃ NOs (3 nm) were exposed to 100 ppm TEA, an extra peak appeared in the wave number range of 2800–3000 cm⁻¹. On the contrary, a minor difference in FTIR spectrum is observed for N-C@ α -Fe₂O₃ NOs (3 nm) (or α -Fe₂O₃ NOs) exposed to other studied interfering gases. Regarding the variation of the FTIR peak at a wave number of 2340 cm⁻¹, it can be attributed to the adsorption of CO₂ during the sample preparation.^{26,41} This interesting finding directly evidences the preferred TEA adsorption on the surface of N-C@ α -Fe₂O₃ NOs (3 nm), that is, TEA adsorption dominates the whole sensing process even on exposing N-C@ α -Fe₂O₃ NOs (3 nm) to a gas mixture. In sum, from the perspective of theoretical analysis, formation of a N-C@ α -Fe₂O₃ NO core–shell heterostructure is helpful in enhancing the humidity resistance and TEA selectivity.

To confirm the assumption, the sensing performance of the sensors composed of α -Fe₂O₃ NOs or N-C@ α -Fe₂O₃ NOs (3 nm) sensing materials is evaluated. Initially, the operating temperature of the sensors is optimized. Figure S6 of the Supporting Information illustrates the variation of response signal to TEA (100 ppm) at different operating temperatures. The maximum response signal is observed for the sensor operated at 250 °C, irrespective of the components of the sensing materials. To give a clearer vision, the transient changes based on the actual R_a value of two sensors vs operating temperature is presented in Figure S7 of the Supporting Information, where R_a values are far below 100 M Ω and meet the practical application. At the optimal operating temperature, the sensor using N-C@ α -Fe₂O₃ NOs (3 nm) exhibits almost 7 times higher response magnitude

than that of the sensor composed of α -Fe₂O₃ NOs, supporting the view of enhancing the response magnitude by designing a core–shell heterostructure. What's more meaningful was that the quantitative relationship between the thickness of the N–C shell and the amount of melamine had also been established, as the thickness of the N–C shell is controllable by tuning the amount of melamine, as shown in Figure S8 of the Supporting Information that the thickness of the shell increased from 3 to 8 nm after increasing the ratio of melamine to α -Fe₂O₃ NOs from 1:1 to 8:1. However, when the mass ratio of melamine to α -Fe₂O₃ NOs reached 10:1, the surface agglomerated obviously, which indicates that the upper limit of a polycondensation film was reached (Figure S9 of the Supporting Information). Besides, the relationship between the N–C shell thickness and the mass ratio of melamine to α -Fe₂O₃ NOs is shown in Table S1. Cross-sensitivity of the sensors composed of α -Fe₂O₃ NOs, N-C@ α -Fe₂O₃ NOs (3 nm), N-C@ α -Fe₂O₃ NOs (5 nm), N-C@ α -Fe₂O₃ NOs (8 nm), and N–C shells was investigated and is presented in Figure 3a. In this study, several toxic industrial chemicals, e.g., nitrobenzene, ammonia, formaldehyde, ethylenediamine, SO₂, and NO₂, which can be usually found near chemical plants are selected as the interfering gas species. Interestingly, in comparison with the sensor using α -Fe₂O₃ NOs or N-C@ α -Fe₂O₃ NOs (3 nm, 8 nm) as the sensing material, the sensor consisting of N-C@ α -Fe₂O₃ NOs (3 nm) shows significant improvement in the response magnitude to TEA due to the synergistic effect of the preferred TEA adsorption and p (N–C shell)–n (α -Fe₂O₃ NOs) junction, while a minor increment is witnessed for other examined interference gases.^{20,42} The response signal to these selected interfering gases is 5–10 times lower than that to TEA at the same level, resulting in essential enhancement in the selectivity. Additionally, the decline in the response magnitude on further increasing the shell thickness indicates that the shell thickness influences the gas reaction greatly, which is probably due to the fact that a

Table 1. Comparison of Sensor Performance of N-C@ α -Fe₂O₃ NOs and α -Fe₂O₃ NOs with Other MOS Sensor Materials for Detection of TEA

materials	LOD (ppm)	operating temperature (°C)	concn (ppm)/res.	res./rec. time (s)	RH (%)	res. vs RH	refs
Al ₂ O ₃ / α -Fe ₂ O ₃ nanofibers	0.5	250	100/15	1/17	20–98	negative	1
SnO ₂ /Au/Fe ₂ O ₃ nanoboxes	0.05	240	100/126.8	7/10			S1
Au/ α -Fe ₂ O ₃ nanorods	1	40	50/17.5	12/8	30–80	negative	S2
α -Fe ₂ O ₃ microrod	10	275	100/11.8	33/70			S3
α -Fe ₂ O ₃ @CuO nanorods	1	40	50/12.8	9/20	10–50	negative	S4
α -Fe ₂ O ₃ @NiO nanorods	1	40	50/12.2	8/19	10–50	negative	S4
Au@SnO ₂ / α -Fe ₂ O ₃ nanoneedles	0.6	300	100/30	4/200			S5
α -Fe ₂ O ₃ NOs	0.56	250	100/2.2	15/300	30–90	negative	this work
N-C@ α -Fe ₂ O ₃ NOs	0.4	250	100/13.8	7/250	30–90	humidity resistant	this work

thick shell extends the gas diffusion pathway, thus limiting the transport of gas molecules and their reaction with the internal nucleus. Specifically, it is reasonable to conclude that the satisfactory response behavior is mainly contributed by α -Fe₂O₃ NOs, since a negligible response signal is generated by the sensor solely using N-C. Besides, the decline of response magnitude after increasing the thickness of the N-C shell proves that a thinner shell is more favorable for gas diffusion. It must be particularly noted that the referred all-vapor-phase processing method plays an important role in coating such a thin shell. In contrast to other reported synthetic approaches, such as the traditional hydrothermal route, electron beam evaporation, magnetron sputtering, and chemical vapor deposition, the synthesis method presented in this article features low cost, simple operation, uniform membrane thickness, and elemental distribution.^{43–47} Hence, the proposed coating method will provide a cost-effective approach to produce thin shells in future sensing applications. Then, transient responses of the sensors composed of α -Fe₂O₃ NOs or N-C@ α -Fe₂O₃ NOs (3 nm) for the TEA concentration within the range of 1–200 ppm in dry air are studied and given in Figure 3b. Both sensors demonstrate fast response when exposed to high concentration (above 20 ppm). Besides, it can be deduced from the results shown in Figure 3c that the response behavior of the sensor using N-C@ α -Fe₂O₃ NOs (3 nm) can be correlated to the vapor concentration of TEA following the conductance model commonly applied to MOS chemiresistive sensors, $S = a[C]^b + 1$,^{48,49} where S is the sensor response value and C is the vapor concentration of TEA. The equation can be rearranged in a logarithm format showing the linear relationship as $\log(S - 1) = b \log(C) + \log(a)$ at certain operating temperatures. Moreover, the detection limit of N-C@ α -Fe₂O₃ NOs (3 nm) to TEA is down to be 400 ppb according to the results shown in Figure 3c, fully meeting the needs of industrial testing in real applications. Note that both sensors composed of α -Fe₂O₃ NOs or N-C@ α -Fe₂O₃ NOs (3 nm) demonstrate satisfactory reproducibility when detecting 100 ppm TEA at 250 °C, maintaining almost unchanged response during six consecutive cycles (Figures 3d and S10 of the Supporting Information).

Finally, the impact of the fluctuation in humidity on the sensing characteristics is investigated. The response signal of the sensor using N-C@ α -Fe₂O₃ NOs (3 nm) to 100 ppm TEA was tested for a wide range of humidity (0–90% RH), as shown in Figures 3e and S11, S12 of the Supporting Information. Impressively, when the RH increases above 30%, the response signal of the sensor consisting of N-C@ α -Fe₂O₃ NOs (3 nm) remains almost constant with a further

increase in RH till the level of 90%. This robustness against humidity change (particularly in the high RH region) helps to develop a sensor for quantitative detection, since humidity effect is always one of the unpredictable factors causing fluctuations. Compared to the performance in dry air, the sensor response under RH of 30% or above shows ca. 40% decrease in magnitude, which is due to the competitive adsorption of water molecules on the surface of sensor materials. This suggests that a more hydrophobic shell is needed to be explored. Note that the operating temperature of 250 °C may also enhance the humidity resistance due to a preferred desorption for water vapor at such a high temperature.⁵⁰ In other words, although minor increment is observed in the contact angle for water droplets, the synergetic effect derived from the high operating temperature and the relatively hydrophobic surface leads to enhanced humidity resistance when sensing TEA. Stability for the sensor is another concerned issue in real applications. Consequently, the sensing performance of the sensors composed of α -Fe₂O₃ NOs and N-C@ α -Fe₂O₃ NOs (3 nm) to 100 ppm TEA is continuously investigated for 1 month. The stability test shown in Figure 3f implies acceptable durability within the examined period. The average values of these sensors for 100 ppm TEA are 13.8 and 2.2, respectively.

Table 1 summarizes the comparison on sensing behavior of the sensors consisting of the proposed N-C@ α -Fe₂O₃ NOs that based on relatively hydrophobic and TEA adsorption-selective core-shell heterostructure and other reported sensing materials. Conclusively, the overall sensing performance of N-C@ α -Fe₂O₃ NOs for detecting TEA is superior to other MOS sensors previously reported (including α -Fe₂O₃ NOs), regarding the sensitivity, LOD, response time, and humidity effect. Specifically, all these pilot results supported the proposed strategy and achieved the expected research objectives. The success of the proposed strategy offers an efficient and convenient approach to modify the sensing properties of the sensor toward the expected research objective.

In view of the above excellent gas sensing performance, particularly, the enhanced humidity resistance, a portable sensing prototype is assembled for remote monitoring of TEA via wireless transmission. As shown in Figure 4a–c, the TEA sensing prototype consists of the circuit in a box with the volume of 200 × 130 × 80 mm³ (width × length × height), and a detection probe based on the sensor comprised of N-C@ α -Fe₂O₃ NOs (3 nm) is placed inside. The operating temperature can be set by adjusting the heating current through the knob. When switch to detecting mode, real-time

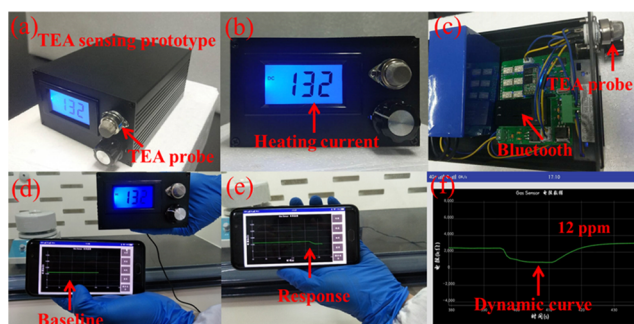


Figure 4. (a–c) Photograph of details for the portable TEA sensing prototype based on the N–C@ α -Fe₂O₃ NOs (3 nm) probe, (d, e) simulated TEA gas testing, and (f) transient dynamic response–recovery curves of the sensing prototype to the simulated TEA atmosphere.

response signal in terms of resistance changes is transmitted via blue-tooth and appeared in the application interface. To demonstrate the availability of the TEA monitor, a simulation experiment was implemented. As can be seen from Figure 4d, a stable baseline appears in the application interface when the probe is placed outside the fume hood, and when the probe is placed inside the fume hood where the TEA gas environment is simulated (under the RH of 70%), the resistance drops significantly (Figure 4e). When the detection probe is taken out, it returns to the background value. Figure 4f shows the dynamic response–recovery curves of the N–C@ α -Fe₂O₃ NOs (3 nm) sensor, and according to the linear fitting equation in Figure 3c, the concentration of TEA in the fume hood is calculated to be 12 ppm which is consistent with the theoretically set value. Conclusively, the developed sensing prototype that based on the N–C@ α -Fe₂O₃ NOs (3 nm) probe can be potentially applied in industrial organic amine detection, even in high humidity.

Regarding the sensing principle, it can be interpreted through the migration of electrons, which plays an important role in the surface oxidization of target organic molecules, thus can affect the response/recovery speeds, sensitivity, or selectivity of the sensor. To have a deeper insight, the energy band diagram of such heterojunction has been particularly analyzed. Figure S13 of the Supporting Information schematically illustrates the electronic band structures of both α -Fe₂O₃ NOs and N–C@ α -Fe₂O₃ NOs (3 nm), and the relevant discussions are presented in the section of materials characterization of the Supporting Information. In summary, an obvious narrowed band gap (E_g) from 1.85 to 1.75 eV and work function (Φ) from 2.95 to 2.75 eV was observed after the effective coating of N–C shell, thus facilitating the transfer of electrons to conduction band (CB) under heating conditions then to oxygen to form more negative ions to enhance the sensing reaction performances. As for the optimal operational temperature at 250 °C observed in the research, thermal gravimetric (TG) combined with FTIR analysis was implemented to understand the reaction progress at different temperatures. In the Supporting Information, the TG curve of N–C@ α -Fe₂O₃ NOs (3 nm) with the decomposition temperatures from 25 to 800 °C under N₂ gas proves a spot of desorption of physically adsorbed H₂O and CO₂ molecules and slight mass loss of N–C Shell via polycondensation of the Supporting Information demonstrate the TG-FTIR results for N–C@ α -Fe₂O₃ NOs (3 nm) pre-treated by saturation

adsorption of TEA with the heating temperatures from 25 to 350 °C (covering the working temperature of the gas sensing test) under N₂ gas, in the wave number of 400–4000 cm⁻¹. These results shown in the Supporting Information suggest that the partial reaction of TEA still maintained a good form of chemi-adsorption on the surface of N–C@ α -Fe₂O₃ NOs at 100 °C, accompanied by a small amount of oxidation. Gradually, with the temperature rising to 350 °C, the remaining TEA was quickly oxidized and exceeded the TEA volatilization rate. In a word, the balance of chemi-adsorption and fast oxidation rate results in the sensor that using N–C@ α -Fe₂O₃ NOs (3 nm) demonstrated optimal sensing performance at the operating temperature of 250 °C.

CONCLUSIONS

Aiming to efficiently enhance the humidity resistance and TEA selectivity of MOS-based chemiresistance sensor, a novel strategy that based on the hydrophobic and TEA adsorption-selective core–shell heterostructure is proposed. To verify the practicability of the proposed strategy, α -Fe₂O₃ NOs that is confirmed to be poorly selective and sensitive to TEA is selected as the core candidate and experimental control. Additionally, N–C@ α -Fe₂O₃ NOs are prepared by a novel, simple, widespread, and controllable evaporating coating method. In comparison with α -Fe₂O₃ NOs, when exposed to TEA an increase in contact angle of water droplets and apparent changes in IR spectrum are observed after coating the N–C shell on the surface of α -Fe₂O₃ NOs core, suggesting a relative hydrophobic and TEA adsorption-selective N–C@ α -Fe₂O₃ NOs core–shell heterostructure. The sensing performance of the sensors using α -Fe₂O₃ NOs or N–C@ α -Fe₂O₃ NOs indicates the fact that the N–C shell indeed modified the sensing characteristics by demonstrating enhanced humidity resistance (within RH 30–90%), selectivity, and sensitivity, as well as LOD to TEA. In particular, a sensing prototype based on the N–C@ α -Fe₂O₃ NOs (3 nm) probe is fabricated and its satisfactory sensing performance further confirmed the potential of its future applications in industrial organic amine detection. These promising results disclose a bright future of enhancing the humidity resistance and selectivity as well as sensitivity of MOS-based chemiresistance sensor by simply adopting a hydrophobic and target gas adsorption (e.g., TEA) preferred core–shell heterostructure.

ASSOCIATED CONTENT

Supporting Information

The Supporting Information is available free of charge at <https://pubs.acs.org/doi/10.1021/acssensors.9b02519>.

Experimental details; materials characterization; illustration of the multistep process of synthesizing N–C@ α -Fe₂O₃ NOs; photograph of the (a) DGL-III humidity control gas and liquid distribution system; (b) CGS-8 intelligent test system; (c) sensing chamber; and (d) sensor unit; TEM image of (a) N–C@ α -Fe₂O₃ NOs (3 nm), selected area electron diffraction image of (b) N–C@ α -Fe₂O₃ NOs (3 nm), (c–f) elemental mapping of Fe, C, O, and N elements in the composite, and EDS spectrum image of (g) N–C@ α -Fe₂O₃ NOs (3 nm); XRD patterns of the (a) as-synthesized α -Fe₂O₃ NOs, (b) N–C@ α -Fe₂O₃ NOs (3 nm), and (c) annealed α -Fe₂O₃ NOs; XPS curves of α -Fe₂O₃ NOs and N–C@ α -Fe₂O₃ NOs (3 nm): (a) the survey spectra of the

samples; (b) the Fe core level (2p) of the samples; (c) O 1s in α -Fe₂O₃ NOs and N-C@ α -Fe₂O₃ NOs; (d) C 1s peak; and (e) N 1s peak in the composite; response of the sensors to 100 ppm of TEA at different working temperatures from 150 to 350 °C; the actual resistance of the sensors to 100 ppm of TEA at different working temperatures from 150 to 350 °C; the actual dynamic resistance changes of the sensors to 100 ppm of TEA at different working temperatures from 150 to 350 °C; (a–d) SEM images of α -Fe₂O₃ NOs, and various N-C@ α -Fe₂O₃ NOs derived from the different ratios of melamine to α -Fe₂O₃ NOs as 1:1, 5:1, and 8:1, respectively, and (e–h) the corresponding HRTEM images of the above samples; SEM images of N-C@ α -Fe₂O₃ NOs derived from the melamine and α -Fe₂O₃ NOs in the ratio of 10:1. Images in (a) and (b) were selected from different areas; the relationship between N-C shell thickness and the mass ratio of melamine and α -Fe₂O₃ NOs; dynamic actual resistance change of α -Fe₂O₃ NOs and N-C@ α -Fe₂O₃ NOs (3 nm)-based sensors to 100 ppm of TEA at 250 °C corresponding to Figure 3d in the article; sensor response profiles of α -Fe₂O₃ NOs and N-C@ α -Fe₂O₃ NOs (3 nm) upon exposure to 100 ppm of TEA under different RHs at 250 °C; sensor resistance profiles of α -Fe₂O₃ NOs and N-C@ α -Fe₂O₃ NOs (3 nm) upon exposure to 100 ppm of TEA under different RHs at 250 °C; sensor resistance profiles of α -Fe₂O₃ NOs and N-C@ α -Fe₂O₃ NOs (3 nm) upon exposure to 100 ppm of TEA under different RHs at 250 °C; (a) optical band gaps determined by UV/Vis diffuse reflectance spectra, (b) secondary electron cutoff (Ecut off) of the UPS, (c) valence band spectra measured by UPS, and (d) schematics illustrating the electronic band structures; (a) TG curve of N-C@ α -Fe₂O₃ NOs (3 nm) with the decomposition temperatures from 25 to 800 °C under N₂ gas, (b) the TG and (c) FTIR combining analysis of N-C@ α -Fe₂O₃ NOs (3 nm) pretreated by saturation adsorption of TEA with the heating temperatures from 25 to 350 °C (covering the working temperature of the gas sensing test) under N₂ gas, in the wave number of 400–4000 cm⁻¹ (PDF)

AUTHOR INFORMATION

Corresponding Authors

Liwei Wang – School of Marine Sciences, Guangxi University, Nanning 530004, China; Guangxi Laboratory on the Study of Coral Reefs in the South China Sea, Nanning 530003, China; Guangxi Key Laboratory of Processing for Nonferrous Metallic and Featured Materials, Nanning 530003, China; Email: wangliwei0427@163.com

Han Jin – Institute of Micro-Nano Science and Technology, Shanghai Jiaotong University, Shanghai 200240, China; Ningbo Materials Science and Technology Institute, Chinese Academy of Sciences, Ningbo 315201, China; The State Key Laboratory of Bioelectronics, Southeast University, Nanjing 210096, China; orcid.org/0000-0001-7427-4600; Email: jinhan10@sjtu.edu.cn

Ling Zang – Nano Institute of Utah and Department of Materials Science and Engineering, University of Utah, Salt Lake City, Utah 84112, United States; Email: lzang@eng.utah.edu

Authors

Hao Fu – School of Marine Sciences, Guangxi University, Nanning 530004, China; Guangxi Laboratory on the Study of Coral Reefs in the South China Sea, Nanning 530003, China; Guangxi Key Laboratory of Processing for Nonferrous Metallic and Featured Materials, Nanning 530003, China

Hongyun Shao – School of Marine Sciences, Guangxi University, Nanning 530004, China; Guangxi Laboratory on the Study of Coral Reefs in the South China Sea, Nanning 530003, China; Guangxi Key Laboratory of Processing for Nonferrous Metallic and Featured Materials, Nanning 530003, China

Dehua Xia – School of Environmental Science and Engineering, Sun Yat-sen University, Guangzhou 510275, China; orcid.org/0000-0001-6016-358X

Shengwei Deng – College of Chemical Engineering, Zhejiang University of Technology, Hangzhou 310014, China

Yinghui Wang – School of Marine Sciences, Guangxi University, Nanning 530004, China; Guangxi Laboratory on the Study of Coral Reefs in the South China Sea, Nanning 530003, China; Guangxi Key Laboratory of Processing for Nonferrous Metallic and Featured Materials, Nanning 530003, China

Yi Chen – School of Information Science and Engineering, Ningbo University, Ningbo 315211, China

Changzhou Hua – School of Information Science and Engineering, Ningbo University, Ningbo 315211, China

Li Liu – Faculty of Information Engineering, Ningbo University of Finance & Economics, Ningbo 315175, Zhejiang, China

Complete contact information is available at:

<https://pubs.acs.org/10.1021/acssensors.9b02519>

Notes

The authors declare no competing financial interest.

ACKNOWLEDGMENTS

This work is supported by the National Natural Science Foundation of China (51762005, 61771267, and 61971250), the Natural Science Foundation of Guangxi Province, China (2017GXNSFAA198254), Science and Technology Project of Guangxi (AD17129063), Science and Technology Major Project of Guangxi (AA17202020, AA17204100, and AA18242007), funding from the State Key Laboratory of Bioelectronics of Southeast University, Natural Science Foundation of Ningbo City (2017A610229 and 2018A610092), Humanity and Social Science Foundation of Chinese Education Department (19YJC880053), the Natural Science Foundation of Zhejiang (LQ18F010008), the Philosophy and Social Science Planning Project of Zhejiang (19NDJC0103YB), and Innovation Project of Guangxi Graduate Education (YCSW2018029).

REFERENCES

- (1) Kou, X.; Xie, N.; Wang, C.; Liang, X.; Liu, F.; Gao, Y.; Chuai, X.; Zhang, H.; Lu, G.; Sun, Y.; et al. Detection of Triethylamine with Fast Response by Al₂O₃/ α -Fe₂O₃ Composite Nanofibers. *Sens. Actuators, B* **2018**, *266*, 139–148.
- (2) Ju, D. X.; Xu, H. Y.; Qiu, Z. W.; Zhang, Z. C.; Xu, Q.; Zhang, J.; Wang, J. Q.; Cao, B. Q. Near Room Temperature, Fast-Response, and Highly Sensitive Triethylamine Sensor Assembled with Au-Loaded ZnO/SnO₂ Core-Shell Nanorods on Flat Alumina Substrates. *ACS Appl. Mater. Interfaces* **2015**, *7*, 19163–19171.

- (3) Zou, Y.; Chen, S.; Sun, J.; Liu, J.; Che, Y.; Liu, X.; Zhang, J.; Yang, D. Highly Efficient Gas Sensor Using a Hollow SnO₂ Microfiber for Triethylamine Detection. *ACS Sens.* **2017**, *2*, 897–902.
- (4) Ma, C.; Wang, L.; Zhang, Y.; Yang, X.; Liang, X.; Hao, X.; Liu, T.; Liu, F.; Yan, X.; Gao, Y.; et al. Mixed-Potential Type Triethylamine Sensor Based on NASICON Utilizing SmMO₃ (M = Al, Cr, Co) Sensing Electrodes. *Sens. Actuators, B* **2019**, *284*, 110–117.
- (5) Akesson, B.; Skerfving, S.; Mattiasson, L. Experimental Study on the Metabolism of Triethylamine in Man. *Occup. Environ. Med.* **2008**, *45*, 262–268.
- (6) Yang, T.; Gu, K.; Zhu, M.; Lu, Q.; Zhai, C.; Zhao, Q.; Yang, X.; Zhang, M. ZnO-SnO₂ Heterojunction Nanobelts: Synthesis and Ultraviolet Light Irradiation to Improve the Triethylamine Sensing Properties. *Sens. Actuators, B* **2019**, *279*, 410–417.
- (7) Liu, S. R.; Guan, M. Y.; Li, X. Z.; Guo, Y. Light Irradiation Enhanced Triethylamine Gas Sensing Materials Based on ZnO/ZnFe₂O₄ composites. *Sens. Actuators, B* **2016**, *236*, 350–357.
- (8) Qu, F.; Shi, E.; Zhang, F.; Shi, S.; Lin, H.; Wang, Q. Enhanced Triethylamine-Sensing Properties of p-n Heterojunction Co₃O₄/In₂O₃ Hollow Microtubes Derived from Metal–Organic Frameworks. *Sens. Actuators, B* **2018**, *262*, 739–749.
- (9) Gu, D.; Li, X.; Zhao, Y.; Wang, J. Enhanced NO₂ sensing of SnO₂/SnS₂ Heterojunction Based Sensor. *Sens. Actuators, B* **2017**, *244*, 67–76.
- (10) Kida, T.; Suematsu, K.; Hara, K.; Kanie, K.; Muramatsu, A. Ultrasensitive Detection of Volatile Organic Compounds by a Pore Tuning Approach Using Anisotropically Shaped SnO₂ Nanocrystals. *ACS Appl. Mater. Interfaces* **2016**, *8*, 35485–35495.
- (11) Fu, H. R.; Wu, X. X.; Ma, L. F.; Wang, F.; Zhang, J. Dual-Emission SG7@MOF Sensor via SC–SC Transformation: Enhancing the Formation of Excimer Emission and the Range and Sensitivity of Detection. *ACS Appl. Mater. Interfaces* **2018**, *10*, 18012–18020.
- (12) Suh, B. L.; Lee, S.; Kim, J. Size-Matching Ligand Insertion in MOF-74 for Enhanced CO₂ Capture under Humid Conditions. *J. Phys. Chem. C* **2017**, *121*, 24444–24451.
- (13) Patel, H. A.; Mansor, N.; Gadipelli, S.; Brett, D. J.; Guo, Z. Superacidity in Nafion/MOF Hybrid Membranes Retains Water at Low Humidity to Enhance Proton Conduction for Fuel Cells. *ACS Appl. Mater. Interfaces* **2016**, *8*, 30687–30691.
- (14) Drobek, M.; Kim, J. H.; Bechelany, M.; Vallicari, C.; Julbe, A.; Sub Kim, S. MOF-Based Membrane Encapsulated ZnO Nanowires for Enhanced Gas Sensor Selectivity. *ACS Appl. Mater. Interfaces* **2016**, *8*, 8323–8328.
- (15) Gao, X.; Li, F.; Wang, R.; Zhang, T. A Formaldehyde Sensor: Significant Role of p-n Heterojunction in Gas-Sensitive Core-Shell Nanofibers. *Sens. Actuators, B* **2018**, *258*, 1230–1241.
- (16) Sharma, A.; Tomar, M.; Gupta, V. A Low Temperature Operated NO₂ Gas Sensor Based on TeO₂/SnO₂ p-n Heterointerface. *Sens. Actuators, B* **2013**, *176*, 875–883.
- (17) Kwon, H.; Yoon, J. S.; Lee, Y.; Kim, D. Y.; Baek, C. K.; Kim, J. K. An Array of Metal Oxides Nanoscale Hetero p-n Junctions toward Designable and Highly-Selective Gas Sensors. *Sens. Actuators, B* **2018**, *255*, 1663–1670.
- (18) Nakate, U. T.; Ahmad, R.; Patil, P.; Wang, Y.; Bhat, K. S.; Mahmoudi, T.; Yu, Y. T.; Suh, E. K.; Hahn, Y. B. Improved Selectivity and Low Concentration Hydrogen Gas Sensor Application of Pd Sensitized Heterojunction n-ZnO/p-NiO Nanostructures. *J. Alloys Compd.* **2019**, *797*, 456–464.
- (19) Dhawale, D. S.; Salunkhe, R. R.; Patil, U. M.; Gurav, K. V.; More, A. M.; Lokhande, C. D. Room Temperature Liquefied Petroleum Gas (LPG) Sensor Based on p-Polyaniline/n-TiO₂ Heterojunction. *Sens. Actuators, B* **2008**, *134*, 988–992.
- (20) Wang, D.; Gu, W.; Zhang, Y.; Hu, Y.; Zhang, T.; Tao, X.; Chen, W. Novel C-Rich Carbon Nitride for Room Temperature NO₂ Gas Sensors. *RSC Adv.* **2014**, *4*, 18003–18006.
- (21) Zhang, Y.; Zhang, Y.; Zhang, D.; Li, S.; Jiang, C.; Su, Y. Confinement Preparation of Au Nanoparticles Embedded in ZIF-67-Derived N-Doped Porous Carbon for High-Performance Detection of Hydrazine in Liquid/Gas Phase. *Sens. Actuators, B* **2019**, *285*, 607–616.
- (22) Li, G.; Zhang, X.; Lu, H.; Yan, C.; Chen, K.; Lu, H.; Gao, J.; Yang, Z.; Zhu, G.; Wang, C.; et al. Ethanol Sensing Properties and Reduced Sensor Resistance Using Porous Nb₂O₅-TiO₂ n-n Junction Nanofibers. *Sens. Actuators, B* **2019**, *283*, 602–612.
- (23) Hu, M.; Kang, W.; Zhong, Z.; Cheng, B.; Xing, W. Porphyrin-Functionalized Hierarchical Porous Silica Nanofiber Membrane for Rapid HCl Gas Detection. *Ind. Eng. Chem. Res.* **2018**, *57*, 11668–11674.
- (24) Qiao, X. Q.; Zhang, Z. W.; Hou, D. F.; Li, D. S.; Liu, Y.; Lan, Y. Q.; Zhang, J.; Feng, P.; Bu, X. Tunable MoS₂/SnO₂ p-n Heterojunctions for an Efficient Trimethylamine Gas Sensor and 4-Nitrophenol Reduction Catalyst. *ACS Sustainable Chem. Eng.* **2018**, *6*, 12375–12384.
- (25) Wang, K.; Qian, X.; Zhang, L.; Li, Y.; Liu, H. Inorganic–Organic p-n Heterojunction Nanotree Arrays for a High-Sensitivity Diode Humidity Sensor. *ACS Appl. Mater. Interfaces* **2013**, *5*, 5825–5831.
- (26) Vladimirova, S. A.; Romyantseva, M. N.; Filatova, D. G.; Chizhov, A. S.; Khmelevsky, N. O.; Konstantinova, E. A.; Kozlovsky, V. F.; Marchevsky, A. V.; Karakulina, O. M.; Hadermann, J.; et al. Cobalt Location in p-CoOx/n-SnO₂ Nanocomposites: Correlation with Gas Sensor Performances. *J. Alloys Compd.* **2017**, *721*, 249–260.
- (27) Liu, X.; Xu, S.; Chi, H.; Xu, T.; Guo, Y.; Yuan, Y.; Yang, B. Ultrafine 1D Graphene Interlayer in g-C₃N₄/Graphene/Recycled Carbon Fiber Heterostructure for Enhanced Photocatalytic Hydrogen Generation. *Chem. Eng. J.* **2019**, *359*, 1352–1359.
- (28) Liu, S.; Wang, S.; Jiang, Y.; Zhao, Z.; Jiang, G.; Sun, Z. Synthesis of Fe₂O₃ Loaded Porous g-C₃N₄ Photocatalyst for Photocatalytic Reduction of Dinitrogen to Ammonia. *Chem. Eng. J.* **2019**, *373*, 572–579.
- (29) Wang, L.; Fu, H.; Jin, Q.; Jin, H.; Haick, H.; Wang, S.; Yu, K.; Deng, S.; Wang, Y. Directly Transforming SnS₂ Nanosheets to Hierarchical SnO₂ Nanotubes: Towards Sensitive and Selective Sensing of Acetone at Relatively Low Operating Temperatures. *Sens. Actuators, B* **2019**, *292*, 148–155.
- (30) Qin, J.; Lai, X.; Liang, S.; Wang, F.; Jiang, X.; Li, J. Highly Sensitive Acetone Gas Sensor Based on Ultrafine α-Fe₂O₃ Nanoparticles. *Sens. Actuators, B* **2016**, *238*, 923–927.
- (31) Cho, I.; Kang, K.; Yang, D.; Yun, J.; Park, I. Localized Liquid-Phase Synthesis of Porous SnO₂ Nanotubes on MEMS Platform for Low-Power, High Performance Gas Sensors. *ACS Appl. Mater. Interfaces* **2017**, *9*, 27111–27119.
- (32) Li, Y. H.; Hung, T. H.; Chen, C. W. A First-Principles Study of Nitrogen and Boron-Assisted Platinum Adsorption on Carbon Nanotubes. *Carbon* **2009**, *47*, 850–855.
- (33) He, L.; Weniger, F.; Neumann, H.; Beller, M. Synthesis, Characterization, and Application of Metal Nanoparticles Supported on Nitrogen-Doped Carbon: Catalysis beyond Electrochemistry. *Angew. Chem., Int. Ed.* **2016**, *55*, 12582–12594.
- (34) Zhao, Y.; Lai, Q.; Wang, Y.; Zhu, J.; Liang, Y. Interconnected Hierarchically Porous Fe, N-Codoped Carbon Nanofibers as Efficient Oxygen Reduction Catalysts for Zn–Air Batteries. *ACS Appl. Mater. Interfaces* **2017**, *9*, 16178–16186.
- (35) Chen, F.; Surkus, A. E.; He, L.; Pohl, M. M.; Radnik, J.; Topf, C.; Junge, K.; Beller, M. Selective Catalytic Hydrogenation of Heteroarenes with N-Graphene-Modified Cobalt Nanoparticles (Co₃O₄-Co/NGr@α-Al₂O₃). *J. Am. Chem. Soc.* **2015**, *137*, 11718–11724.
- (36) Su, D. S.; Perathoner, S.; Centi, G. Nanocarbons for the Development of Advanced Catalysts. *Chem. Rev.* **2013**, *113*, 5782–5816.
- (37) Zhang, L.; Wang, A.; Wang, W.; Huang, Y.; Liu, X.; Miao, S.; Liu, J.; Zhang, T. Co–N–C Catalyst for C–C Coupling Reactions: On the Catalytic Performance and Active Sites. *ACS Catal.* **2015**, *5*, 6563–6572.
- (38) Basu, A. K.; Chauhan, P. S.; Awasthi, M.; Bhattacharya, S. α-Fe₂O₃ Loaded RGO Nanosheets Based Fast Response/Recovery CO Gas Sensor at Room Temperature. *Appl. Surf. Sci.* **2019**, *465*, 56–66.

(39) Jian, Y.; Yu, T.; Jiang, Z.; Yu, Y.; Douthwaite, M.; Liu, J.; Albilali, R.; He, C. In-Depth Understanding of the Morphology Effect of α -Fe₂O₃ on Catalytic Ethane Destruction. *ACS Appl. Mater. Interfaces* **2019**, *11*, 11369–11383.

(40) Zhang, X.; Niu, Y.; Meng, X.; Li, Y.; Zhao, J. Structural Evolution and Characteristics of the Phase Transformations between α -Fe₂O₃, Fe₃O₄ and γ -Fe₂O₃ Nanoparticles under Reducing and Oxidizing Atmospheres. *CrystEngComm* **2013**, *15*, 8166–8172.

(41) Hieu, N.; Van, Nguyen, L. C.; Thu, N. T. A.; Nam, P. C.; Cuong, N. D.; Khieu, D. Q.; Toan, N.; Van, Hung, C. M. Fe₂O₃ Nanoporous Network Fabricated from Fe₃O₄/Reduced Graphene Oxide for High-Performance Ethanol Gas Sensor. *Sens. Actuators, B* **2017**, *255*, 3275–3283.

(42) Babu, P.; Mohanty, S.; Naik, B.; Parida, K. Serendipitous Assembly of Mixed Phase BiVO₄ on B-Doped g-C₃N₄: An Appropriate p-n Heterojunction for Photocatalytic O₂ Evolution and Cr(VI) Reduction. *Inorg. Chem.* **2019**, *58*, 12480–12491.

(43) Kozak, A. O.; Porada, O. K.; Ivashchenko, V. I.; Ivashchenko, L. A.; Scrynsky, P. L.; Tomila, T. V.; Manzhara, V. S. Comparative Investigation of Si-C-N Films Prepared by Plasma Enhanced Chemical Vapour Deposition and Magnetron Sputtering. *Appl. Surf. Sci.* **2017**, *425*, 646–653.

(44) Pan, G. X.; Cao, F.; Zhang, Y. J.; Xia, X. H. Integrated Carbon Cloth Supported LiFePO₄/N-C Films as High-Performance Cathode for Lithium Ion Batteries. *Mater. Res. Bull.* **2018**, *98*, 70–76.

(45) Chen, H.; Shen, K.; Mao, Q.; Chen, J.; Li, Y. Nanoreactor of MOF-Derived Yolk-Shell Co@C-N: Precisely Controllable Structure and Enhanced Catalytic Activity. *ACS Catal.* **2018**, *8*, 1417–1426.

(46) Morton, K. C.; Tokuhisa, H.; Baker, L. A. Pyrolyzed Carbon Film Diodes. *ACS Appl. Mater. Interfaces* **2013**, *5*, 10673–10681.

(47) Blackstock, J. J.; Rostami, A. A.; Nowak, A. M.; McCreery, R. L.; Freeman, M. R.; McDermott, M. T. Ultraflat Carbon Film Electrodes Prepared by Electron Beam Evaporation. *Anal. Chem.* **2004**, *76*, 2544–2552.

(48) Williams, D. E. Semiconducting Oxides as Gas-Sensitive Resistors. *Sens. Actuators, B* **1999**, *57*, 1–16.

(49) Xu, Z.; Duan, G.; Zhang, H.; Wang, Y.; Xu, L.; Cai, W. In Situ Synthesis of Porous Array Films on a Filament Induced Micro-Gap Electrode Pair and Their Use as Resistance-Type Gas Sensors with Enhanced Performances. *Nanoscale* **2015**, *7*, 14264–14271.

(50) Zhang, S.; Lei, T.; Li, D.; Zhang, G.; Xie, C. UV Light Activation of TiO₂ for Sensing Formaldehyde: How to Be Sensitive, Recovering Fast, and Humidity Less Sensitive. *Sens. Actuators, B* **2014**, *202*, 964–970.

(51) Liu, L.; Zhao, Y.; Song, P.; Yang, Z.; Wang, Q. Ppb Level Triethylamine Detection of Yolk-Shell SnO₂/Au/Fe₂O₃ Nanoboxes at Low-Temperature. *Appl. Surf. Sci.* **2019**, *476*, 391–401.

(52) Song, X.; Xu, Q.; Zhang, T.; Song, B.; Li, C.; Cao, B. Room-Temperature, High Selectivity and Low-Ppm-Level Triethylamine Sensor Assembled with Au Decahedrons-Decorated Porous α -Fe₂O₃ Nanorods Directly Grown on Flat Substrate. *Sens. Actuators, B* **2018**, *268*, 170–181.

(53) Sun, G.; Chen, H.; Li, Y.; Ma, G.; Zhang, S.; Jia, T.; et al. Synthesis and Triethylamine Sensing Properties of Mesoporous α -Fe₂O₃ Microrods. *Mater. Lett.* **2016**, *178*, 213–216.

(54) Xu, Q.; Zhang, Z.; Song, X.; Yuan, S.; Qiu, Z.; Xu, H.; Cao, B. Improving the Triethylamine Sensing Performance Based on Debye Length: A Case Study on α -Fe₂O₃ @NiO(CuO) Core-Shell Nanorods Sensor Working at near Room-Temperature. *Sens. Actuators, B* **2017**, *245*, 375–385.

(55) Xu, H.; Li, W.; Han, R.; Zhai, T.; Yu, H.; Chen, Z.; Wu, X.; Wang, J.; Cao, B. Enhanced Triethylamine Sensing Properties by Fabricating Au@SnO₂/ α -Fe₂O₃ Core-Shell Nanoneedles Directly on Alumina Tubes. *Sens. Actuators, B* **2018**, *262*, 70–78.